



Deposited via The University of Leeds.

White Rose Research Online URL for this paper:

<https://eprints.whiterose.ac.uk/id/eprint/105683/>

Version: Accepted Version

Article:

Oloyede, O, Cochrane, RF and Mullis, AM (2017) Effect of rapid solidification on the microstructure and microhardness of BS1452 grade 250 hypoeutectic grey cast iron. *Journal of Alloys and Compounds*, 707. pp. 347-350. ISSN: 0925-8388

<https://doi.org/10.1016/j.jallcom.2016.08.214>

© 2016 Elsevier B.V. Licensed under the Creative Commons Attribution-NonCommercial-NoDerivatives 4.0 International <http://creativecommons.org/licenses/by-nc-nd/4.0/>

Reuse

Items deposited in White Rose Research Online are protected by copyright, with all rights reserved unless indicated otherwise. They may be downloaded and/or printed for private study, or other acts as permitted by national copyright laws. The publisher or other rights holders may allow further reproduction and re-use of the full text version. This is indicated by the licence information on the White Rose Research Online record for the item.

Takedown

If you consider content in White Rose Research Online to be in breach of UK law, please notify us by emailing eprints@whiterose.ac.uk including the URL of the record and the reason for the withdrawal request.

Effect of rapid solidification on the microstructure and microhardness of BS1452 grade 250 hypoeutectic grey cast iron.

Olamilekan Oloyede^{1, a}, Robert F. Cochrane¹, Andrew M. Mullis¹

¹Institute for Material Research, University of Leeds, Leeds LS2-9JT, UK

^aCorresponding author: pmoro@leeds.ac.uk

Abstract

Containerless solidification of low alloyed commercial grey cast iron in two different cooling media (N₂ and He) using a 6.5 m high vacuum drop-tube have been investigated. Both the conventionally cooled, as-cast alloy and the rapidly cooled drop-tube samples were characterized using SEM, XRD and Vickers microhardness apparatus. The estimated range of cooling rates are 200 K s⁻¹ to 16,000 K s⁻¹ for N₂ cooled droplets and 700 K s⁻¹ to 80,000 K s⁻¹ for He cooled droplets (in each case for 850 μm and 38 μm diameter droplets respectively). Microstructural analysis reveals that the as-received bulk sample displayed a graphitic structure while the rapidly cooled samples display decreasing amounts of α-Fe as the cooling rate increases. At moderate cooling rates α is replaced with γ and Fe₃C, while at higher cooling rates with α'. Microhardness increase with cooling rate but cannot be mapped uniquely onto cooling rate, suggesting undercooling also influences the mechanical properties.

Keywords: Containerless solidification; Metastable phase; Grey cast iron; Microstructure; Microhardness

1. Introduction

Conventional solidification, as might occur for instance in a casting, is invariably initiated by heterogeneous nucleation at very low undercooling (typically 1-2 K). In contrast, during non-equilibrium solidification, as might occur within a population of fine droplets during gas atomization, undercoolings of 10's or even 100's of Kelvin may be experienced depending upon the particle size and cooling rate, which is itself primarily a function of particle size, atomizing medium and gas velocity [1-2]. This study investigates the changes in morphology of grey cast iron as a function of droplet size at constant composition and compares the rapidly solidified material against an as-cast control sample. Two different cooling media, N₂ and He, are used in the study, which allows some separation of the effects of cooling rate and droplet undercooling.

Grey cast iron stands out as one of the most widely used metallic materials because of its superior properties such as good castability, machinability and formability, high damping capacity, relative low cost and good corrosion resistance [3]. Normally, the microstructure of conventionally cooled grey cast iron comprises free carbon, in the form of graphite flakes, in a ferrite – pearlite matrix. The principal effects of graphite flakes, which form only during slow cooling, is to reduce the strength and toughness of the product, the graphite acts as an easy pathway for crack propagation. However, there are a number of ways to inhibit graphite formation in cast iron, one of which is through rapid solidification processing, for instance through High-Pressure Gas Atomization (HPGA). However, in this study, drop-tube processing, which is an analogue of HPGA, was used.

Very limited investigations on the rapid solidification of grey cast iron have been undertaken to date. Hsu et al. [4] improved the fracture toughness of grey iron alloyed with Cu by austempering, with the increase in fracture toughness increasing with retained austenite in the microstructure of the alloy. Hemanth [5], investigated the effect of cryogenic and water quenching on microstructure and mechanical properties of cast iron. Their results show that cooling rate has a marked effect on secondary dendrite arm spacing and grain size, which affects the ultimate tensile strength and fracture toughness of the final product. Bartocha et al. [6], worked on the qualitative and quantitative analysis of graphite in grey cast iron and the effect of graphite morphologies and casting condition on the mechanical properties of grey iron, allowing them to correlate improved properties in the alloy with microstructural changes as a function of solidification conditions. Likewise, Özdemir et al. [7], revealed the effect of graphite shape on the diffusion bonding of grey cast iron and this they found has many parallels to solidification processing. Yang et al. [8], in a study of gas atomized grey cast iron powders, related

the microstructural evolution of the powders to the particle size (and hence cooling rate). They showed that with increasing cooling rate there was a change in the flake morphology from random to oriented. Moreover, from their XRD analysis it was evident that with increasing cooling rate (decreasing particle size) the proportion of γ -Fe increased while that of α -Fe decreased. However, there was no evidence, either from their XRD or microstructural analysis, of any phases other than ferrite, austenite and Fe_3C . In a study by Yi et al. [9], based on repair technology using the rapid solidification process by laser fusion welding, they discovered that overall crack toughness of the material can be increased around the repaired zone (RZ). This was further explained by Ebrahimmia et al. [10] who stated that cracks initiate mostly at the interface of graphite and then propagate through the matrix of a component thereby causing fracture.

2. Experimental

The composition of the as-cast sample used for this study, together with the ASTM standard specification, is shown in Table 1, confirming the materials to be a hypoeutectic cast iron with Carbon Equivalent (CE) of 3.70%. This as-cast material, obtained from West Yorkshire Steel, was used as feedstock for the drop-tube experiments and also served as a reference material against which the effects of rapid solidification could be evaluated. The rapidly solidified droplets were produced using a 6.5 m drop-tube, which was filled to a pressure of 50 kPa with dried, oxygen free N_2 or He gas. The corresponding cooling rate for the largest (850 μm) and smallest (38 μm) droplets were estimated as 200 K s^{-1} to 16,000 K s^{-1} for N_2 and 700 K s^{-1} to 80,000 K s^{-1} for He respectively, this difference being mainly due to the higher thermal conductivity of He.

Prior to melt processing the tube was evacuated to ~ 1 Pa and then flushed with the appropriate gas at 50 kPa, this process being repeated 3 times. The tube was then evacuated to 4×10^{-4} Pa before being filled with 50 kPa of either N_2 or He gas. Thereafter, weighed pieces of the as-cast sample were loaded into an alumina crucible with 3 laser drilled holes (approx. 300 μm in diameter) in the base. The sample was heated by induction heating of a graphite susceptor surrounding the crucible. An R-type thermocouple was inserted in the crucible to monitor the melt temperature and when the desired superheat was reached the melt was ejected by pressurising the crucible with 300 kPa of either N_2 or He gas. **Fig. 1** shows the estimated cooling rate as a function of droplet size for the two media. The droplets produced were then sieved into 9 standard sizes and hot mounted using Transoptic resin for XRD analysis and SEM characterization. Vickers microhardness indentation measurements were also made on the mounted and polished samples, with at least 10 measurements of HV0.05 being made in each case. Further details of the experimental procedure are given in Ref. [11].

Table 1: Elemental composition of commercial grey cast iron BS1452 grade 250 analysed by XRF method.

Element (wt.%)	C	Si	Mn	P	S	Fe	CE
ASTM specification	2.5-4.0	1.0-3.0	0.2-1.0	0.002-1.0	0.02-0.025	96.28-90.96	Cal.
BS1452 grade 250	2.70	2.83	0.58	0.148	0.054	93.34	3.70

3. Results and discussions

The result of selected XRD analyses are displayed in **Fig. 2**, revealing the constituent phases present in 300 μm and 53 μm droplets cooled in N_2 and He. Also given, for reference, is the corresponding analysis for the as-received material. From the XRD data it is evident that the as-cast sample is composed predominately of α ferrite (graphite is also present but the peaks occur for $2\theta < 20^\circ$). With increasing cooling rate (300 μm N_2) it is clear that retained γ (austenite) also becomes a constituent phase, together with Fe_3C (cementite), which most likely coexists with α in the form of pearlite. With yet further increases in cooling rate (53 μm N_2 , 300 μm He) α appears to be transforming to α' (Martensite), a transformation that appears essentially complete at the highest cooling rates studied (53 μm He).

The SEM micrograph of the as-cast alloy is as shown in **Fig. 3**. It reveals type A graphite flakes randomly distributed in a ferritic – pearlitic matrix; which is consistent with the slow cooling rate likely to have been

encountered during formation. However, for the rapidly solidified samples, a range of distinct morphological changes may be identified based on the particle size and cooling medium, as shown in **Fig. 4**. Even droplets with the lowest cooling rate processed (N_2 cooled 850 μm diameter droplets, not shown) have a quite different microstructure from that of the conventionally cooled, as-cast sample, this mainly being evident by the absence of flake graphite. At moderate cooling rate (**Fig. 4a**, 300 μm N_2) the dominant microstructural feature is that of an interconnected network of dendritic austenite, with interdendritic pearlite. With increasing cooling rate (**Fig. 4b&c**, 53 μm N_2 & 300 μm He) the microstructure develops a lath type morphology consistent with the occurrence of α' in the XRD patterns, with a refinement of the structural scale of the laths evident at the highest cooling rates (**Fig. 4d**, 53 μm He).

Fig. 5 shows the measured values of the Vickers microhardness plotted against the calculated cooling rate in the two media. For cooling rates $< 5000 K s^{-1}$ the data for the N_2 -cooled and He-cooled droplets lie broadly on the same curve. This is as expected if cooling rate is the prime factor determining the microhardness of the samples. However, for cooling rates $> 5000 K s^{-1}$ the data departs from lying on a single curve, with the data for the N_2 -cooled droplets lying significantly above that for He-cooled droplets. The likely explanation for this is that the microhardness of the droplets is being controlled not only by their cooling rate but also by their undercooling prior to nucleation. Undercooling in small droplets is determined both by the cooling rate the droplet is subject to and by its size. The latter is due to the melt sub-division effect [12], with small droplets likely to contain fewer potent heterogeneous nuclei than large droplets. Consequently, small droplets will experience a larger undercooling than large droplets, even where the cooling rate is similar. In the case of the data presented here, to obtain a cooling rate of $5000 K s^{-1}$, a droplet falling through N_2 would need to be 90 μm in diameter while one falling through He could be up to 220 μm in diameter, with the smaller size of the N_2 cooled droplet meaning it will undercool more. Consequently, the separation of the N_2 and He microhardness curves is likely to reflect the higher undercooling attained in the smaller, N_2 cooled droplets. Moreover, the difference is large, at a cooling rate of $16,000 K s^{-1}$ (the highest achieved for N_2), the N_2 -cooled samples are estimated to be $\sim 150HV_{0.05}$ harder than the He-cooled droplets experiencing the same cooling rate. Although the effect of cooling rate on the mechanical properties of cast iron have been the subject of previous investigations, particularly for transformations in the solid-state this is, as far as we are aware, one of the first demonstrations of the effect of undercooling on said mechanical properties. Microstructural features that are influenced primarily by undercooling, rather than cooling rate, and which might lead to a change in mechanical properties include primary dendrite arm spacing.

4. Conclusions

With rapid solidification processing, there are obvious morphological changes in hypoeutectic grey cast iron with complete disappearance of graphite flakes in all the droplets and a progressive transformation of α -Fe to retained γ -phase and finally to α' -Fe with increase in cooling rate. At constant droplet size He-cooled samples experienced higher cooling rate because of the better thermal conductivity of He and thereby exhibit higher microhardness values as compared to the correspondingly sized sample cooled in N_2 . However, at constant cooling rate, for cooling rates above $5000 K s^{-1}$, the N_2 cooled droplets display higher microhardness values, a consequence of higher undercooling in the smaller droplets. As such this is one of the first demonstrations of the effect of undercooling on the mechanical properties of grey cast iron.

Acknowledgement

This study was carried out in the Institute for Materials Research, University of Leeds, UK. The authors acknowledged the support of Dianne Cochrane, Stuart Micklethwaite and Michael Ward for their assistance with sample preparation and microscopy. Oloyede Olamilekan acknowledges financial support from Federal Government of Nigeria through PTDF.

References

- [1] J. Gao, and B. Wei, Containerless solidification of undercooled NdFeZrB alloy droplets in drop tube, J. Alloy. Compd. 285.1 (1999) 229-232.

- [2] A.M. Mullis, L. Farrell, R.F. Cochrane, Estimation of cooling rate during close-coupled gas atomization using secondary dendrite arm spacing measurement, *Metall. Mater. Trans. B* 44.4 (2013) 992-999.
- [3] C.F. Walton, and T.J. Opar, *Iron casting handbook covering data on Grey, Malleable and ductile iron*, (1981) Iron castings handbook. Iron Castings Society, Inc, New York.
- [4] C.H. Hsu, Y.H. Shy, Y.H. Yu, and S.C. Lee, Effect of austempering heat treatment on fracture toughness of copper alloyed gray iron, *Mater. Chem. Phys.* 63.1 (2000) 75 – 81.
- [5] J. Hemanth, Effect of sub-zero (cryogenic) and water-cool chilling on solidification and mechanical behaviour of cast iron, *J. Mater. Sci. Eng. A* 318.1 (2001) 244 – 253.
- [6] D. Bartocha, K. Janerka and J. Suchoń, Charge materials and technology of melt and structure of gray cast iron, *J. Mater. Process. Technol.*, 162 (2005) 465 – 470.
- [7] N. Özdemir, M. Aksoy and N. Orhan, Effect of graphite shape in vacuum-free diffusion bonding of nodular cast iron with gray cast iron, *J. Mater. Process. Technol.*, 141.2 (2003) 228 – 233.
- [8] M. Yang, Y. Dai, C. Song and Q. Zhai, Microstructure evolution of grey cast iron powder by high pressure gas atomization, *J. Mater. Process. Technol.* 210 (2010) 351 – 355.
- [9] P. Yi, P. Xu, C. Fan, G. Yang, D. Liu and Y. Shi, Microstructure Formation and Fracturing Characteristics of Grey Cast Iron Repaired Using Laser, *The Scientific World Journal* 2014 (2014) 541569.
- [10] M. Ebrahimnia, F.M. Ghaini, Sh. Gholizade and M. Salari, Effect of cooling rate and powder characteristics on the soundness of heat affected zone in powder welding of ductile cast iron *Materials & Design*, 33 (2012) 551 – 556.
- [11] O. Oloyede, T.D. Bigg, R.F. Cochrane & A.M. Mullis, Microstructure evolution and mechanical properties of drop-tube processed, rapidly solidified grey cast iron, *Mater. Sci. Eng. A* 654 (2016) 143 – 150.
- [12] L. Cao, R.F. Cochrane and A.M. Mullis, Solidification morphology and phase selection in drop-tube processed Ni-Fe-Si intermetallics, *Intermetallics* 60 (2015) 33 – 44.

List of Figures

Fig. 1. Estimated cooling rate of droplets cooled in N₂ and He as a function of their diameter.

Fig. 2. X-Ray diffraction traces for: As-cast materials and examples of large (300 μm diameter) and small (53 μm diameter) droplets cooled in both N₂ and He. With increasing cooling rate the dominant phase changes from α (ferrite) in the as-received sample to γ (retained austenite) and Fe₃C (cementite) at moderate cooling rate to α' (Martensite or acicular ferrite) at high cooling rates.

Fig. 3. SEM micrographs of the as-cast alloy, revealing large, randomly oriented, graphite flakes in pearlitic matrix.

Fig. 4. SEM micrographs of rapidly solidified, drop-tube processed samples: (a) 300 μm size fraction cooled in N₂, (b) 53 μm size fraction cooled in N₂, (c) 300 μm size fraction cooled in He and (d) 53 μm size fraction cooled in He.

Fig. 5. Microhardness values (HV0.05) as a function of cooling rate for the different droplet size cooled in N₂ and He.

Figure 1

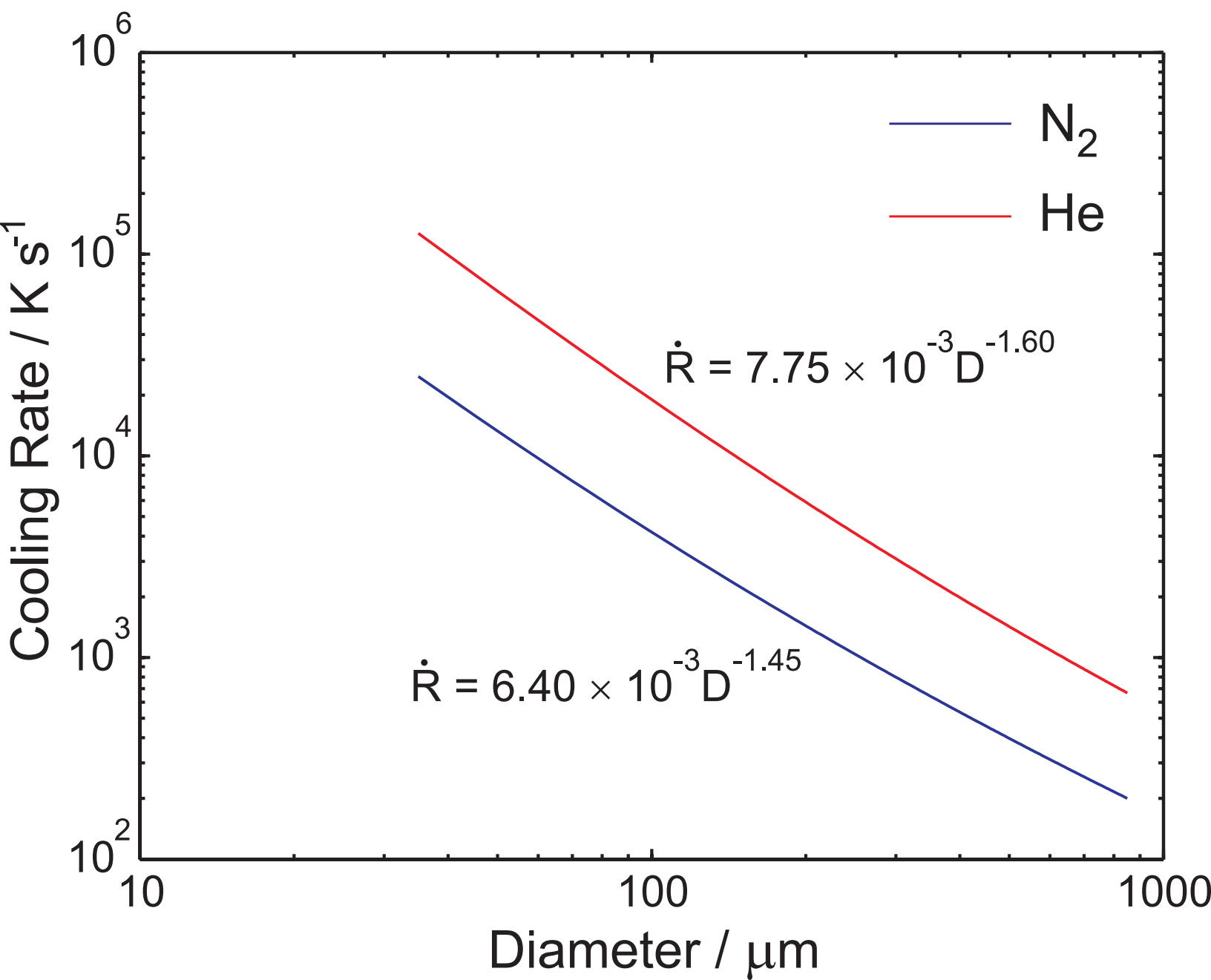


Figure 2

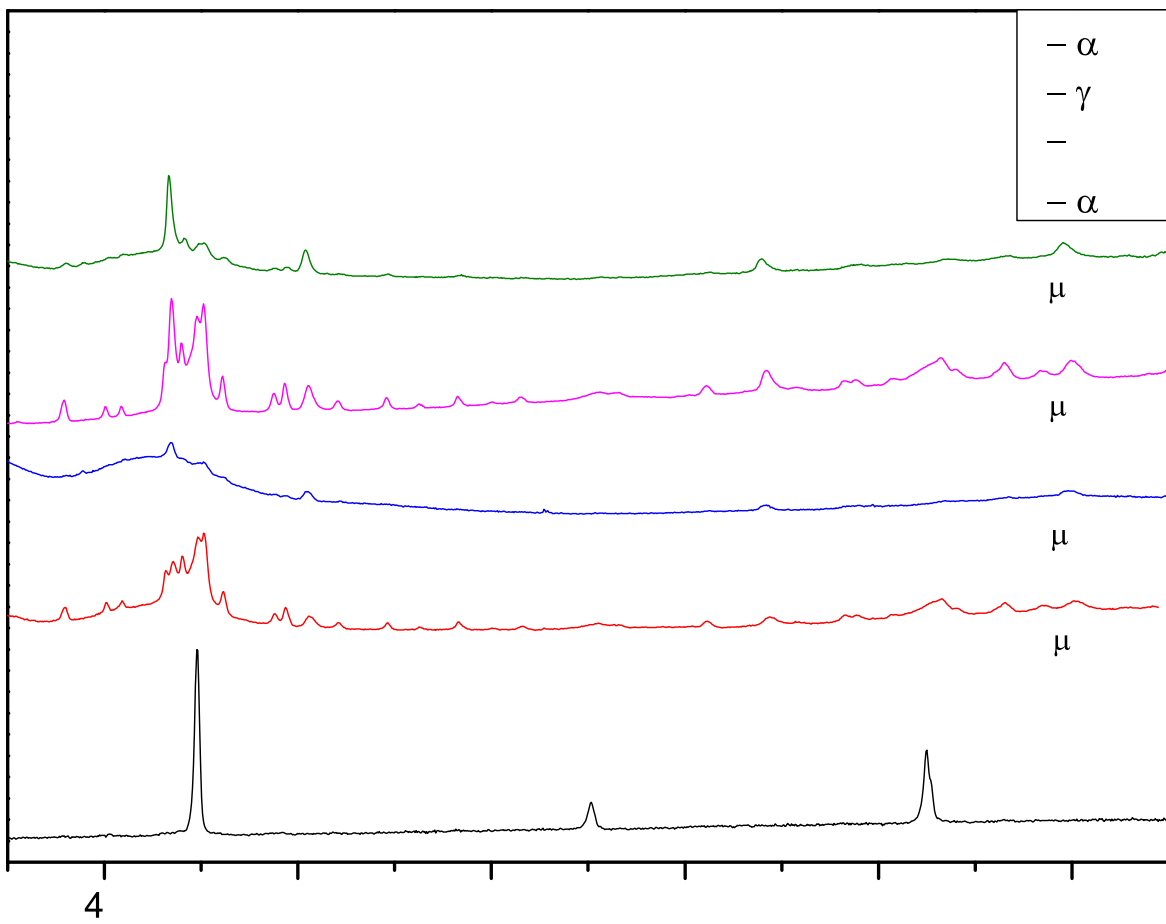


Figure 3

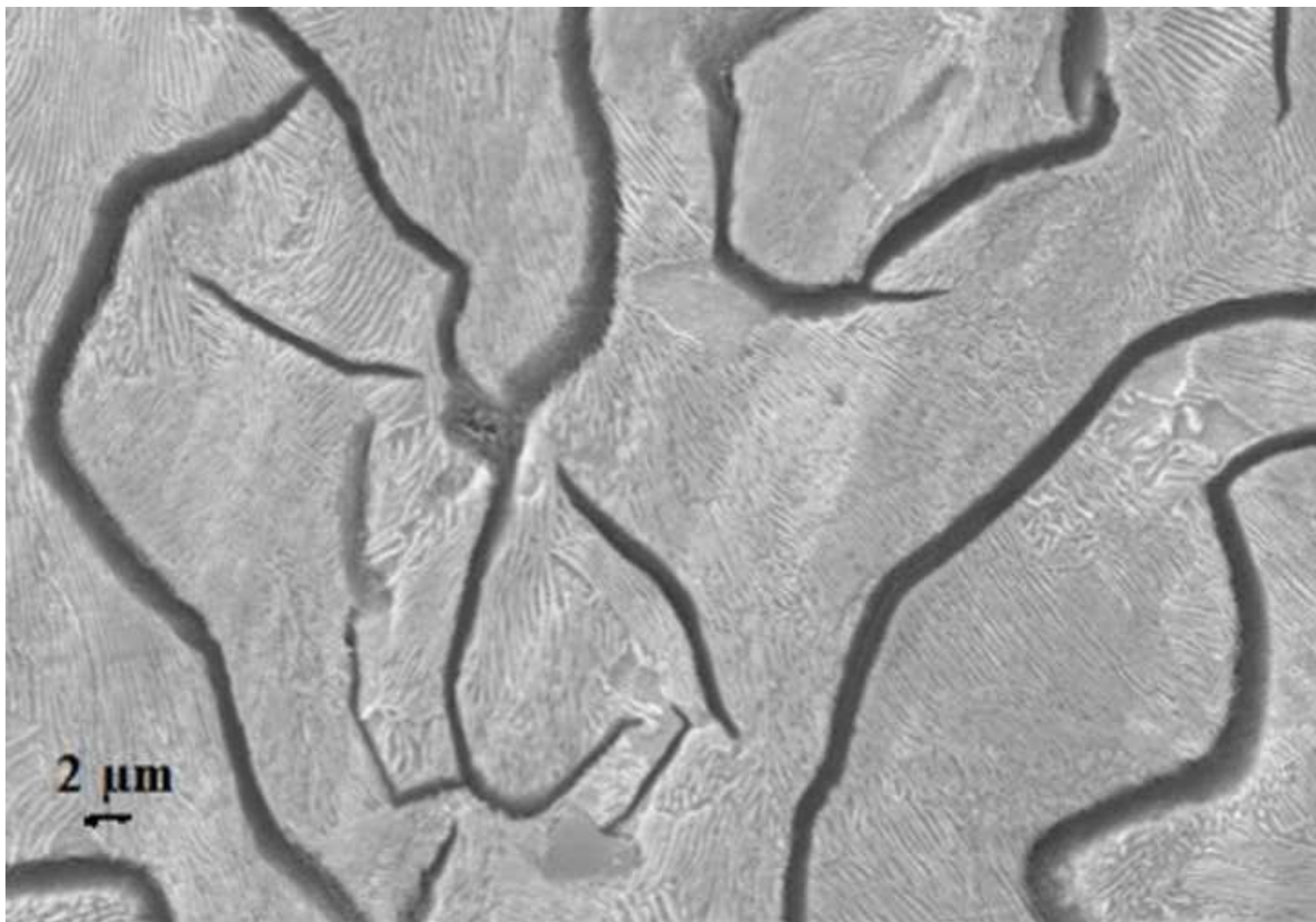


Figure 4

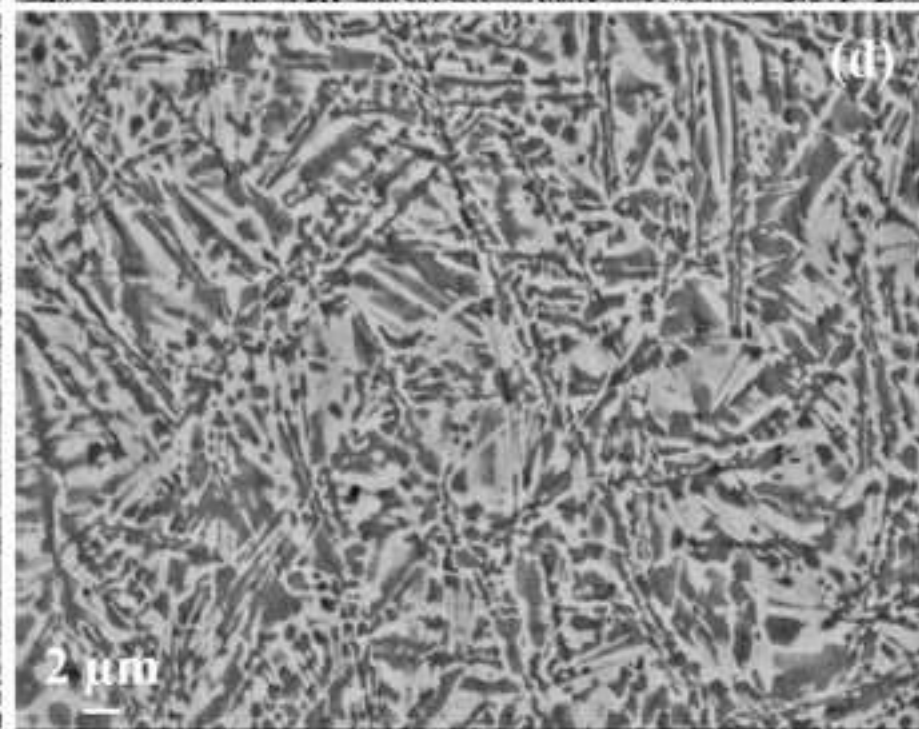
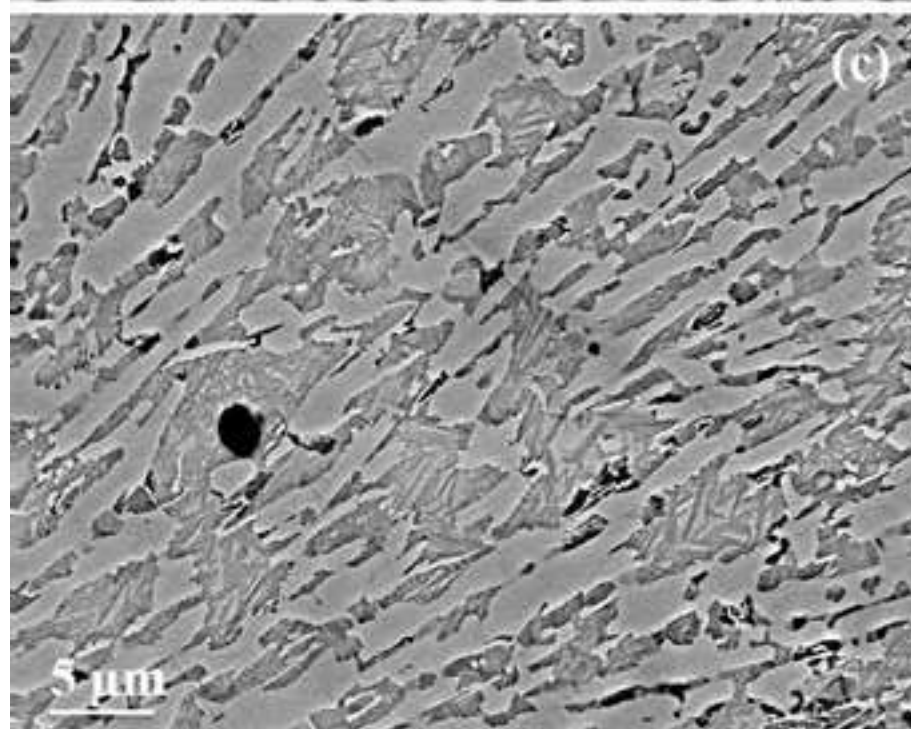
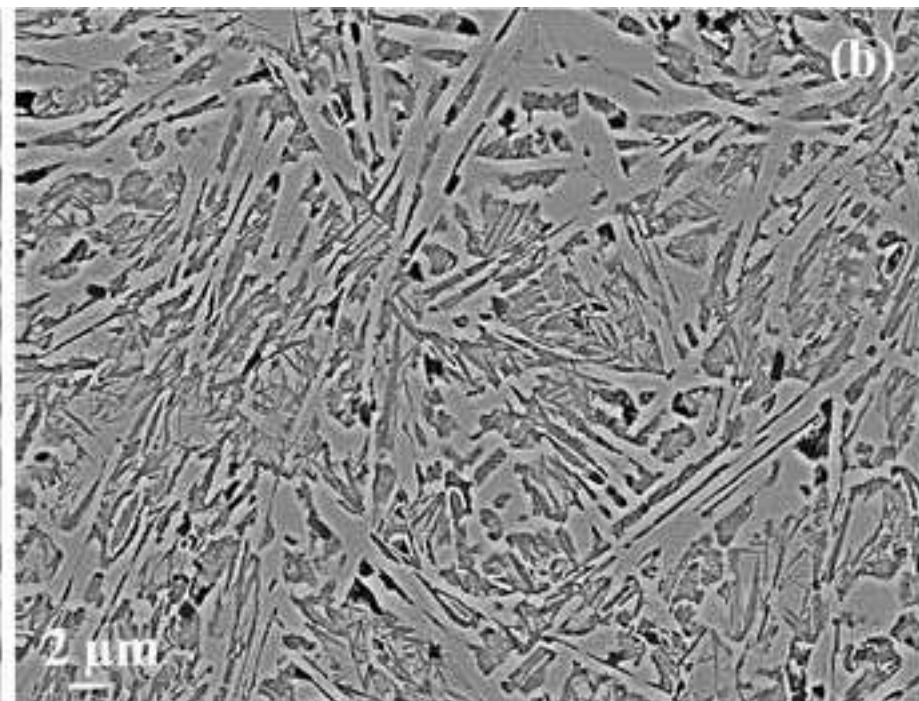
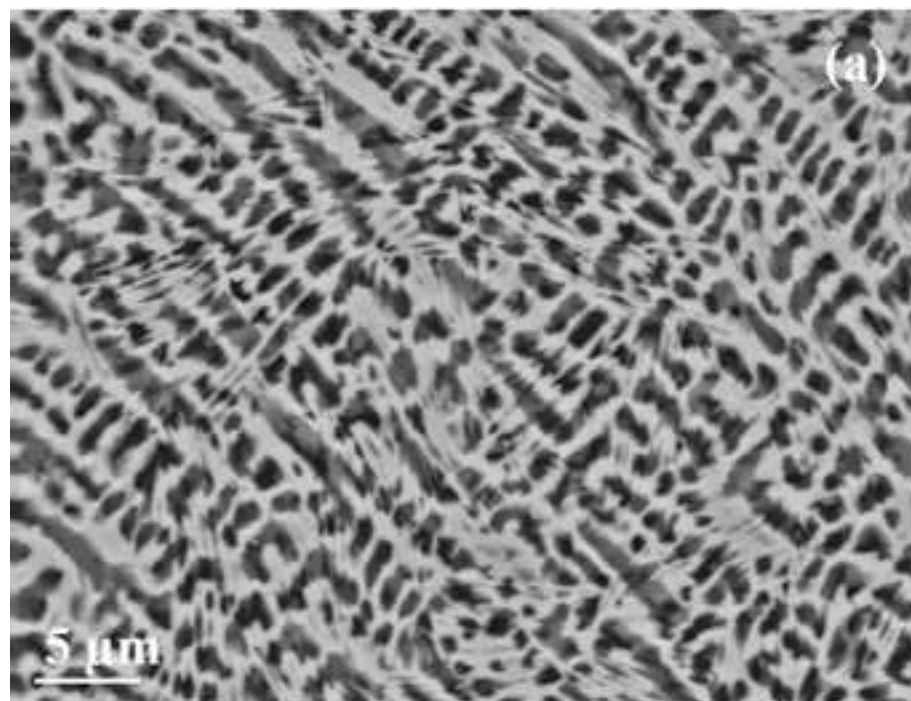


Figure 5

